# Nonlinear Soil-Structure Interaction Analysis Based on the Boundary-Element Method in Time Domain with Application to Embedded Foundation

J.P. Wolf, G.R. Darbre
*Electrowatt Engineering Services Ltd., Bellerivestr. 36, CH-8022 Zurich, Switzerland*

Abstract

The computational procedure of the so-called truncated indirect boundary-element method is derived. The latter, which is non-local in space and time, represents a rigorous generally applicable procedure for taking into account a layered halfspace in a nonlinear soil-structure interaction analysis. As an example, the nonlinear soil-structure interaction analysis of a structure embedded in a halfspace with partial uplift of the basemat and separation of the side wall is investigated.

## 1. Introduction

Nonlinear soil-structure interaction analysis is presented in detail in Reference 1. For a surface foundation, the so-called indirect boundary-element method is described in Reference 2, where Green's functions in the time domain are used for the layered halfspace. In the present paper the formulation is expanded to an embedded foundation. As discussed in Reference 1, the calculation is based on the free-field motion determined for the linear soil. The free field consists of the continuous layered halfspace without any excavation. The motion has to be determined only on the surface which later on will form the structure-soil interface. In contrast, in the system ground (which actually represents the subsystem of the soil), the excavated part is not present. The corresponding motion is referred to as scattered motion.

## 2. Truncated Indirect Boundary-Element Method

The structure-soil interface S of the embedded foundation is discretised using boundary elements compatible with the adjacent finite-element model of the structure. The nodes located on S are denoted as b. In Figure 1, the nomenclature used is illustrated for the in-plane motion, i.e. for two dimensions. It is straightforwardly extended to three dimensions.

The formulation for the nth step leading from time $(n-1)\Delta t$, where all variables are known, to time $n\Delta t$ proceeds as follows. The displacements $\{u(s,t')\}_n$ on S containing the three elements $u(s,t')_n$, $v(s,t')_n$ and $w(s,t')_n$ in the directions of the co-ordinate axes x, y, z (Figure 1b) are introduced first. In the expressions above, the subscript n denotes the nth time step, t' indicates the time measured from the start of this time step ($0 \leq t' \leq \Delta t$) and s represents symbolically a location on S. Introducing the shape functions [N(s)],

$\{u(s,t')\}_n$ is formulated as

$$\{u(s,t')\}_n = [N(s)]\ \{u_b(t')\}_n \tag{1}$$

where $\{u_b(t')\}_n$ denotes the displacements of the nodes b relative to the specified scattered motion $\{u_b^g(t')\}_n$

$$\{u_b(t')\}_n = \{u_b^t(t')\}_n - \{u_b^g(t')\}_n \tag{2}$$

The superscripts t and g refer to the total and scattered motions, respectively. In an explicit algorithm, $\{u_b(t')\}_n$ can be calculated from the known motion at $(n-1)\Delta t$ (central-difference operator).

In the indirect formulation, a fictitious loading pattern acting on that part of the free field which does not form the system ground is introduced. These loads $\{p(s',t')\}_n$ with the three components $p(s',t')_n$, $q(s',t')_n$ and $r(s',t')_n$ are assumed to act on the source surface S' (see Figure 1). S' is always offset towards the soil region to be excavated, in the limiting case by an infinitesimal amount. The loads act on the dynamic system of the free field consisting of the continuous soil, i.e. on the layered halfspace without excavation. The source loads assumed to be constant over each time step (see Figure 2a) are specified as

$$\{p(s',t')\}_n = [L(s')]\ \{p\}_n \tag{3}$$

$\{p\}_n$ are the loads of the nth time step acting in nodes on S', which are, in principle, independent of those on the structure-soil interface, and $[L(s')]$ represents the selected interpolation functions, with s' denoting a location on S'. The number of parameters in $\{p\}_n$ has to be larger than or equal to that in $\{u_b\}_n$. Discontinuities can be introduced as shown in Figure 1c, and time variations other than the selected constant one could be used in equation (3) (see Reference 2 for a linear time variation).

In the indirect formulation, the displacements and tractions caused by the source loads have to be calculated at any time t on the surface S, which subsequently will form the structure-soil interface. For $t = (j-1)\Delta t+\tau'(j\leq n)$ the displacements $\{u_p(s,\tau')\}_j$ are written as

$$\{u_p(s,\tau')\}_j = \sum_{i=1}^{j} [g_u(s,\tau')]_{j-i}\ \{p\}_i \tag{4}$$

where $[g_u(s,\tau')]_{j-i}$ represents the Green's functions for the displacements caused by unit nodal source loads acting during the ith time step. The time variation of one component of $[g_u(s,\tau')]_{j-i}$ is schematically shown in Figure 2b. Analogously, the corresponding surface tractions $\{t_p(s,\tau')\}_j$ with the components $t_{px}(s,\tau')_j$, $t_{py}(s,\tau')_j$ and $t_{pz}(s,\tau')_j$ (Figure 1b) are formulated as

$$\{t_p(s,\tau')\}_j = \sum_{i=1}^{j} [g_t(s,\tau')]_{j-i}\ \{p\}_i \tag{5}$$

As only a finite number of load intensities can be introduced at distinct time steps, the displacement boundary condition on the structure-soil interface S cannot be satisfied exactly by the displacements caused by the source loads (i.e. in every point on S for every t), but only in an average sense as

$$\sum_{j=1}^{n} \int_0^{\Delta t} \int_S [W(s,\tau')]^T_{n-j}\ (\{u_p(s,\tau')\}_j - \{u(s,\tau')\}_j)\ ds\ d\tau' = 0 \tag{6}$$

The matrix $[W(s,t')]_{n-j}$ denotes the weighting functions applicable to the jth time step. Various choices are possible for $[W(s,\tau')]_{n-j}$. In the truncated indirect boundary-element method, it is selected as non-zero for the nth time step only (i.e. for j = n) and equal to the matrix of the Green's functions for the surface tractions

$$[W(s,t')]_o = [g_t(s,\Delta t-t')]_o \tag{7}$$

Then, equation (6) is transformed to

$$\int_o^{\Delta t} \int_S [g_t(s,\Delta t-t')]_o^T (\{u_p(s,t')\}_n - \{u(s,t')\}_n) ds\, dt' = 0 \tag{8}$$

which represents an integral over the nth time step only. Substituting equations (4) (formulated for j = n) and (1) in equation (8) leads to

$$\sum_{i=1}^{n} [G]_{n-i} \{p\}_i = \{\tilde{u}_b\}_n \tag{9}$$

where

$$[G]_{n-i} = \int_o^{\Delta t} \int_S [g_t(s,\Delta t-t')]_o^T [g_u(s,t')]_{n-i} ds\, dt' \tag{10}$$

$$\{\tilde{u}_b\}_n = \int_o^{\Delta t} \int_S [g_t(s,\Delta t-t')]_o^T [N(s)] ds \{u_b(t')\}_n dt' \tag{11}$$

$[G]_{n-i}$ is the generalised flexibility matrix. Moving the known values to the right-hand side, equation (9) is rewritten as

$$[G]_o \{p\}_n = \{\tilde{u}_b\}_n - \{D\}_n \tag{12}$$

with

$$\{D\}_n = \sum_{i=1}^{n-1} [G]_{n-i} \{p\}_i \tag{13}$$

From virtual work considerations, the concentrated loads at time $n\Delta t$ are obtained as

$$\{R_b\}_n = \int_S [N(s)]^T \{t_p(s,t' = \Delta t)\}_n ds \tag{14}$$

Substituting equation (5) formulated for j=n in equation (14) results in

$$\{R_b\}_n = \sum_{i=1}^{n} [T]_{n-i}^T \{p\}_i \tag{15}$$

where

$$[T]_{n-i} = \int_S [g_t(s,t' = \Delta t)]_{n-i}^T [N(s)] ds \tag{16}$$

In contrast to a surface foundation (Reference 2), the source loads of all previous time steps contribute to the concentrated loads at time $n\Delta t$ for an embedded foundation. Solving equation (12) for $\{p\}_n$ and substituting in equation (15) finally results in

$$\{R_b\}_n = [T]_o^T [G]_o^{-1} \{\tilde{u}_b\}_n - [T]_o^T [G]_o^{-1} \{D\}_n + \sum_{i=1}^{n-1} [T]_{n-i}^T \{p\}_i \tag{17}$$

To gain further physical insight, $\{u_b(t')\}_n$ is expressed, as an example, as

$$\{u_b(t')\}_n = f_o(t') \{u_b\}_n + f_1(t') \{\dot{u}_b\}_n + f_2(t') \{\ddot{u}_b\}_n \tag{18}$$

with known functions $f_i(t')$ (i = 0,1,2). Substituting equation (18) in equation (11) then leads to

$$\{\tilde{u}_b\}_n = [U]_o \{u_b\}_n + [U]_1 \{\dot{u}_b\}_n + [U]_2 \{\ddot{u}_b\}_n \tag{19}$$

where

$$[U]_i = \int_o^{\Delta t} \int_S [g_t(s,\Delta t-t')]_o^T [N(s)]\, ds\, f_i(t')\, dt' \tag{20}$$

Equation (19) transforms equation (17) to

$$\{R_b\}_n = [S_{bb}]_o \{u_b\}_n + [T]_o^T [G]_o^{-1} [U]_1 \{\dot{u}_b\}_n + [T]_o^T [G]_o^{-1} [U]_2 \{\ddot{u}_b\}_n - [T]_o^T [G]_o^{-1} \{D\}_n + \sum_{i=1}^{n-1} [T]_{n-i}^T \{p\}_i \tag{21}$$

with the instantaneous stiffness matrix $[S_{bb}]_o$ defined as

$$[S_{bb}]_o = [T]_o^T [G]_o^{-1} [U]_o \tag{22}$$

This formulation should be compared to the ones for the computational procedure of a surface foundation in the time domain (Reference 2) and of an embedded foundation in the frequency domain (Figure 11 of Reference 3).

## 3. Embedded Foundation with Separation of Side Wall and Uplift of Basemat

As an example, the simple structure shown in Figure 3 having a cylindrical foundation embedded in an elastic halfspace, is examined for a vertical earthquake. In the area of contact between the structure and the soil, it is assumed that no tension can arise. This leads to a local nonlinearity consisting of the partial separation of the side wall and of the partial uplift of the basemat.

The structure, which represents a typical nuclear-reactor building, is modelled by a single degree of freedom in the vertical direction with a fixed-base frequency of 10 Hz. The mass $m_s$ of the structure equals $50 \cdot 10^6$ kg and that of the base, $m_o$, $25 \cdot 10^6$ kg. The ratio of the viscous damping of the structure equals .05. The rigid cylindrical base of depth h = 10 m and radius a = 20 m is embedded in the visco-elastic halfspace having a shear-wave velocity $c_s$ = 500 m/sec, a mass density $\rho = 2.4 \cdot 10^3$ kg/m³ (which results in a shear modulus $G = .6 \cdot 10^9$ N/m²), Poisson's ratio $\nu$ = .33 and a hysteretic damping ratio $\zeta$ = .05. The control motion of the vertically propagating waves is defined at the free surface and consists of an artificial time history of 10 sec duration with a response spectrum which closely follows that of the US-NRC Regulatory Guide 1.60 normalised to .27g.

The equations of motion in the time domain are formulated as (Figure 3)

$$\begin{bmatrix} m_s & 0 \\ 0 & m_o \end{bmatrix} \begin{Bmatrix} \ddot{w}_s^t(t) \\ \ddot{w}_o^t(t) \end{Bmatrix} + \begin{bmatrix} c & -c \\ -c & c \end{bmatrix} \begin{Bmatrix} \dot{w}_s^t(t) \\ \dot{w}_o^t(t) \end{Bmatrix} + \begin{bmatrix} k & -k \\ -k & k \end{bmatrix} \begin{Bmatrix} w_s^t(t) \\ w_o^t(t) \end{Bmatrix} = \begin{Bmatrix} 0 \\ -R_o(t) \end{Bmatrix} \tag{23}$$

where $w_s^t(t)$ and $w_o^t(t)$ are the total vertical displacements of the mass point and the base, respectively. $R_o(t)$ is the interaction force of the soil. The structure's spring and dashpot coefficients are denoted as k and c.

The structure-soil interface is discretised with 10 boundary elements: the side wall with 5 cylinders of equal height and the basemat with 5 annular rings of equal area. The

nodes b are selected in the centres of the boundary elements, where the radial and vertical components of the displacements $\{u_b(t)\}$ are introduced. The shape functions $[N(s)]$ applicable to the boundary elements are selected as piecewise constant over each element.

The truncated indirect boundary-element method is used. To calculate $R_o(t)$ from the interaction forces $\{R_b(t)\}$ equilibrium is formulated as

$$R_o(t) = \{A\}^T \{R_b(t)\} \tag{24}$$

where the vector of kinematic transformation $\{A\}$ contains only zeroes and ones. The source line S' is offset from the structure-soil interface S by an infinitesimal amount, and the nodes associated with the loading coincide with those of the boundary elements. Over each source with the same dimension as the adjacent boundary element, the two components of the loads are constant, and thereby $[L(s')]$ is defined.

As the soil is assumed to remain elastic, the scattered motion $\{u_b^g(t)\}$ can be calculated from that of the free field $\{u_b^f(t)\}$ working in the frequency domain (Reference 4). While only vertical components will arise in $\{u_b^f(t)\}$, $\{u_b^g(t)\}$ contains, in general, radial and vertical components.

The computational procedure for the nth time step (from $(n-1)\Delta t$ to $n\Delta t$) proceeds as follows. The discussion can be restricted to the analysis of the base and the adjacent soil. All variables are known up to time $(n-1)\Delta t$. From the total motion at the centre of the basemat at time $(n-1)\Delta t$, the vertical displacement in the same point at time $n\Delta t$ $(w_o^t)_n$ is calculated. The displacements of the nodes b relative to the scattered motion are thus determined as

$$\{u_b\}_n = \{A\}(w_o^t)_n - \{u_b^g\}_n \tag{25}$$

where $\{A\}$ is discussed in connection with equation (24). The interaction forces, formulated according to the truncated indirect boundary-element method, follow from equation (17). If tension arises for the components of $\{R_b\}_n$ in the direction normal to the structure-soil interface, the corresponding boundary elements of the soil lose contact with the adjacent base of the structure. For the corresponding nodes, the normal and tangential components of the forces are then set equal to zero, which modifies $\{R_b\}_n$. This also affects the source-load parameters $\{p\}_n$. Solving equation (15) for $\{p\}_n$ leads to

$$\{p\}_n = ([T]_o^T)^{-1} \left(- \sum_{i=1}^{n-1} [T]_{n-i}^T \{p\}_i + \{R_b\}_n\right) \tag{26}$$

This modified $\{p\}_n$ is used in all subsequent time steps, while the modified $\{R_b\}_n$ is used to calculate $(R_o)_n$ (equation (24)), which represents the resulting contribution of the soil's interaction forces to the equilibrium equation of the centre of the basemat. This completes the calculation of the nth time step when an explicit integration scheme is used. The use of an implicit scheme requires iterations before proceeding to the next time step.

In all calculations using the boundary-element approach, an implicit scheme with a time step $\Delta t$ = .001 sec is chosen.

To be able to make comparisons, a linear analysis in the frequency domain based on the indirect boundary-element method is performed (Reference 3), using the same spatial discretisation. As an example of an intermediate result, the dynamic-stiffness coefficient in the

vertical direction of the rigid foundation is presented in Figure 4. This coefficient $S^f_{oo}$ refers to the system free field, i.e. to the continuous soil. It is equal to the sum of the coefficients of the system ground $S^g_{oo}$ and of the excavated part of the soil $S^e_{oo}$

$$S^f_{oo} = S^g_{oo} + S^e_{oo} \tag{27}$$

$S^f_{oo}$ is nondimensionalised as

$$S^f_{oo} = K(k+i\, a_o c) \tag{28}$$

where the static-stiffness coefficient K is equal to 7.64 Ga, and where $a_o$ denotes the dimensionless frequency defined as

$$a_o = \omega\, a/c_s \tag{29}$$

and k and c are the spring and damping coefficients. The high-frequency behaviour can easily be determined under the assumption of waves radiating normal to the structure-soil interface. This asymptotic behaviour, obtained by substituting Hankel's asymptotic expansions valid for large arguments, is plotted as a dashed line in Figure 4. The agreement is good.

For purpose of checking, a linear analysis is also performed working exclusively in the time domain using the truncated indirect boundary-element formulation. The results agree extremely well with those obtained in the frequency domain (within 3%). The computational effort is, however, increased by two orders of magnitude.

As an example of the temporal variations of Green's functions the vertical displacement $g_u(\bar{t})$ and the vertical surface traction $g_t(\bar{t})$ in the upper of the two Gauss points of integration of the 3rd boundary element indicated in Figure 3 are plotted in Figure 5. They are due to a vertical unit source load acting on the same source element. The dimensionless time $\bar{t}$ is introduced as

$$\bar{t} = t\, c_s/a \tag{30}$$

The initial value and the initial slope in the time domain ($\bar{t} = 0^+$) can be checked by using the corresponding asymptotic values in the frequency domain ($a_o \to \infty$) (Reference 5). The influence of the arrival of the shear wave travelling across the foundation is clearly visible at $\bar{t} = 2$.

The displacements of the scattered motion $\{u^g_b(t)\}$ in the vertical and radial directions in the centre of element 1 shown in Figure 3 are presented in Figure 6. The radial component is, as expected, small.

The final results of the nonlinear analysis are addressed next. The first 2.5 sec of the time histories of the total acceleration $\ddot{w}^t_s(t)$ of the mass point representing the structure and of the spring force of the structure are shown in Figures 7 and 8. Compared to the results of the linear analysis, the calculation taking uplift and separation into account results in a slightly larger response and exhibits somewhat higher frequencies. As can be seen from the time history of the number of boundary elements which lose contact as presented in Figure 9, a strong nonlinear behaviour occurs.

Finally, the stability of the algorithm is briefly discussed. To reduce the computational effort, it is tempting, in the truncated indirect boundary-element method, to retain only a limited number of terms in the two discretised convolution integrals on the right-hand side of equation (21). Besides decreasing the accuracy, this also affects the stability behaviour.

This is verified in Figure 10, where the time history of the interaction force $R_0(t)$ is examined. The smaller the number of retained terms, the earlier the algorithm becomes unstable.

REFERENCES


1 J.P. Wolf and P. Obernhuber, 'Nonlinear soil-structure-interaction analysis using dynamic stiffness or flexibility of soil in time domain', Earthquake eng. struct. dyn. 13 (1985).

2 J.P. Wolf and P. Obernhuber, 'Non-linear soil-structure-interaction analysis using Green's function of soil in time domain', Earthquake eng. struct. dyn. 13 (1985).

3 J.P. Wolf and G.R. Darbre, 'Dynamic-stiffness matrix of soil by the boundary-element method: conceptual aspects', Earthquake eng. struct. dyn. 12, 385-400 (1984).

4 J.P. Wolf, 'Dynamic Soil-Structure Interaction', Prentice-Hall, Englewood Cliffs, New Jersey, 1985.

5 J.P. Wolf and G.R. Darbre, 'Time-domain boundary-element methods in visco-elasticity with application to a spherical cavity', Proceedings of the 7th International Conference on Boundary Element Methods in Engineering, Como, September 1985.


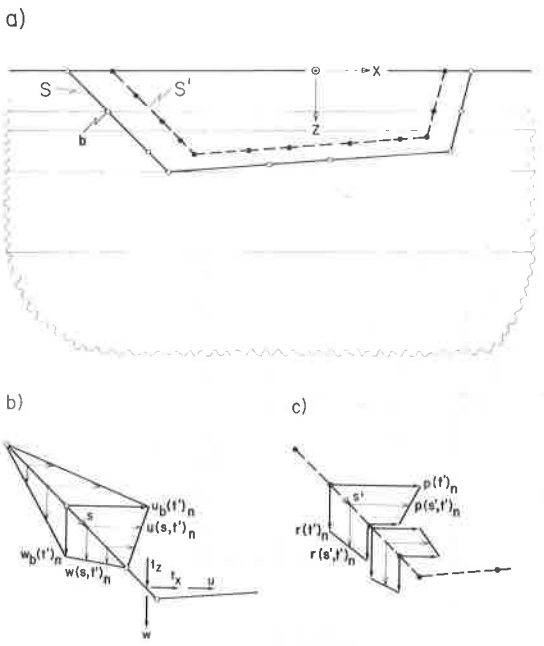


Fig. 1 - Elements of discretisation
(a) source surface and structure-soil interface;
(b) specified displacements; and
(c) selected load distribution

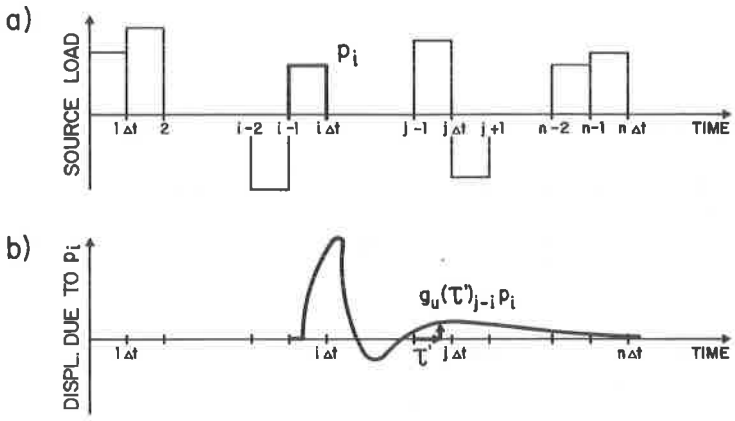


Fig. 2 - Time variations of
(a) source loads; and
(b) Green's function

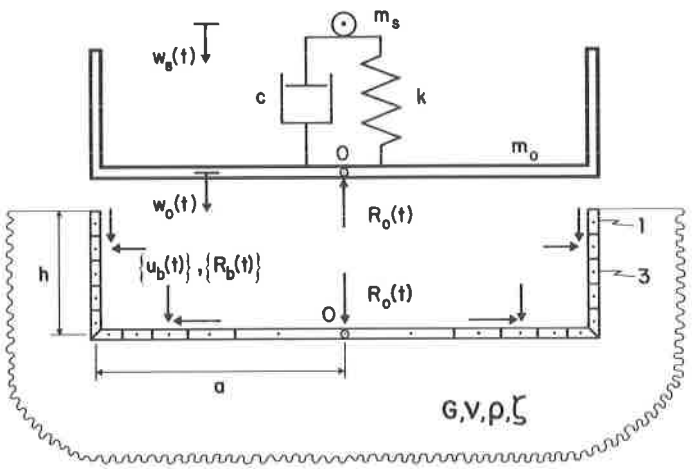


Fig. 3 - Discretised structure-soil system

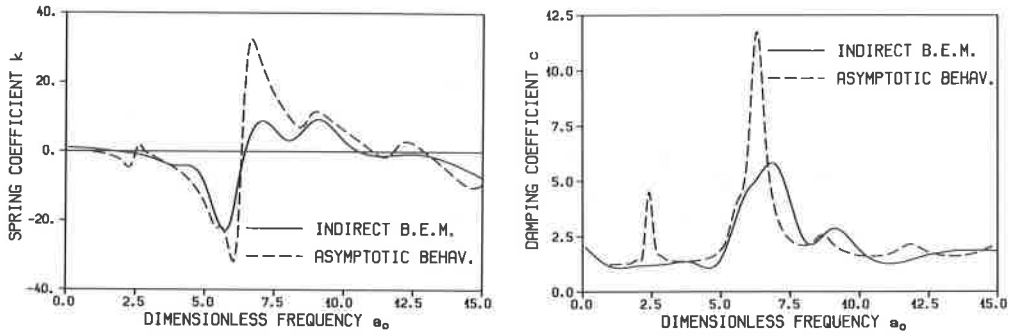


Fig. 4 - Vertical dynamic-stiffness coefficient of free field

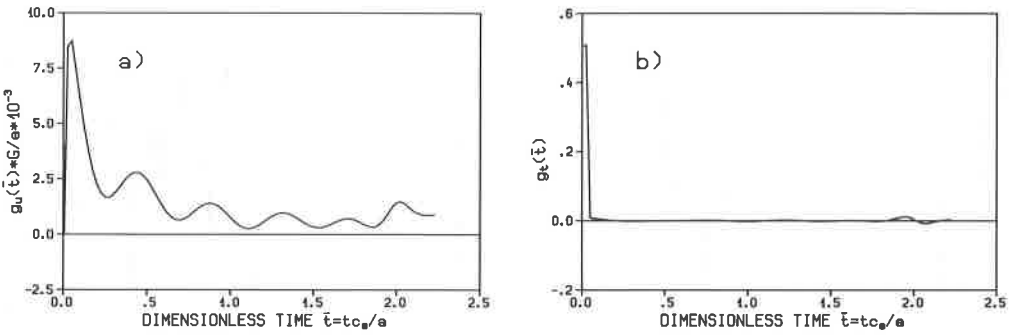


Fig. 5 - Green's functions in time domain
(a) displacement; and (b) surface traction

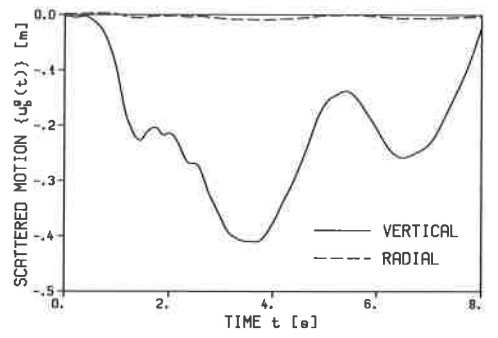


Fig. 6 - Vertical and radial displacements of scattered motion

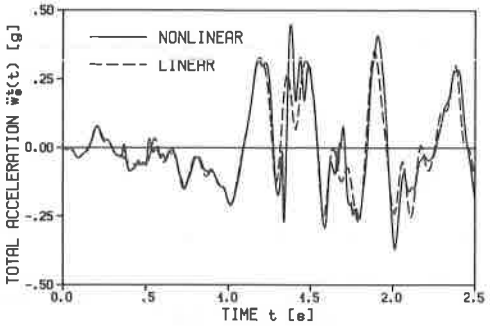


Fig. 7 - Total acceleration of mass

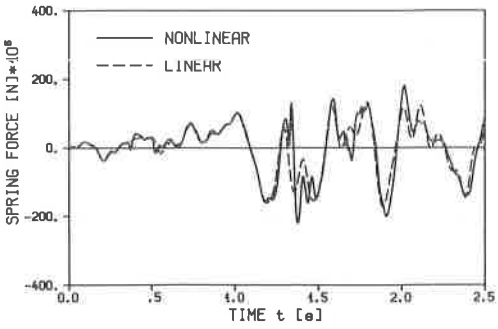


Fig. 8 - Spring force

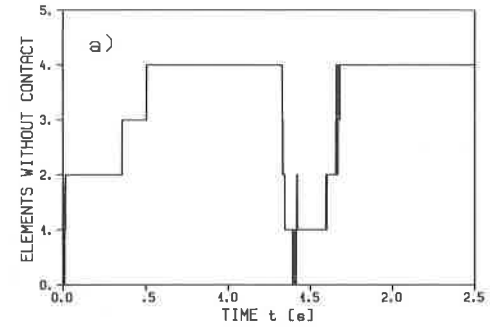


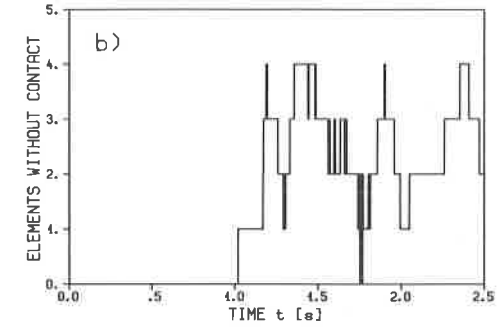


Fig. 9 - Number of boundary elements with loss of contact

a) vertical elements on side wall

b) horizontal elements on basemat

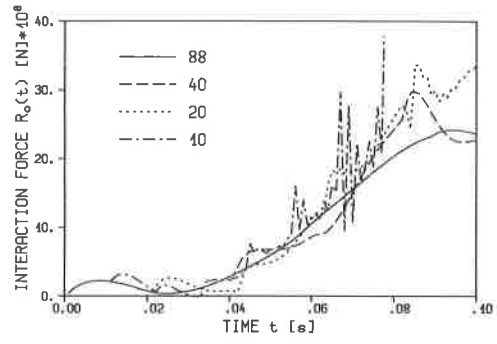


Fig. 10 - Stability behaviour as a function of number of retained terms in convolution integrals